

Liquid Hopfield model: retrieval and localization in heterogeneous liquid mixtures

Rodrigo Braz Teixeira

*Department of Physics, Faculty of Sciences, University of Lisbon, Lisbon, Portugal and
Institute Gulbenkian of Science, Oeiras, Portugal, [equal contribution]*

Giorgio Carugno

*Department of Mathematics, King's College London, Strand,
London, WC2R 2LS, United Kingdom, [equal contribution]*

Izaak Neri

Department of Mathematics, King's College London, Strand, London, WC2R 2LS, United Kingdom

Pablo Sartori

Institute Gulbenkian of Science, Oeiras, Portugal.

(Dated: November 3, 2023)

Biological mixtures, such as the cellular cytoplasm, are composed of a large number of different components. From this heterogeneity, ordered mesoscopic structures emerge, such as liquid phases with controlled composition. These structures compete with each other for the same components. This raises several questions, such as what types of interactions allow the *retrieval* of multiple ordered mesoscopic structures, and what are the physical limitations for the retrieval of said structures. In this work, we develop an analytically tractable model for liquids capable of retrieving states with target compositions. We name this model the *liquid Hopfield model* in reference to corresponding work in the theory of associative neural networks. By solving this model, we show that non-linear repulsive interactions are necessary for retrieval of target structures. We demonstrate that this is because liquid mixtures at low temperatures tend to transition to phases with few components, a phenomenon that we term *localization*. Taken together, our results demonstrate a trade-off between retrieval and localization phenomena in liquid mixtures.

I. INTRODUCTION

Within cells thousands of different components, including proteins, nucleic acids and small peptides, interact with each other [1, 2]. From this heterogeneous mixture, mesoscopic scale ordered structures are *retrieved* to perform specific biological functions. Examples of such retrieval are the assembly of solid-like multi-protein complexes [3], demixing of liquid droplets in the cytoplasm [4–7], or formation of lipid rafts on the membrane [8, 9]. Therefore, the parsimonious coexistence of heterogeneity and order is an essential characteristic of cellular mixtures.

Conventional statistical mechanics and soft matter physics focuses on systems in which the number of component species, N , is much smaller than the total number of components per species, M . The standard thermodynamic limit is thus $N \ll M$ and $M \rightarrow \infty$. In contrast, biological mixtures often take place in the regime $N, M \rightarrow \infty$, and exhibit ordered phases in which the number of components enriched is also large, $Q \lesssim N$. This alternative thermodynamic limit, elsewhere referred to as multifarious [3, 10], is key for the concurrence of heterogeneity and order in biological matter.

Previous studies of liquid mixtures with many components can be roughly grouped in two categories. The first, pioneered by Sear and Cuesta [1], uses analytical tools to study stability of the homogeneous state of a mixture with random interactions [1, 11–15]. The second, uses

numerical inverse optimization on the interactions so to enforce stability of multiple target phases [16, 17]. Both approaches, however, have important caveats: the stability properties of the homogeneous phase cannot be used to predict the properties of ordered phases, which are in any case unlikely for random interactions; and while inverse optimization guarantees by construction stability of target phases it sheds no light into the nature of the interactions that guarantee such stability. Due to these limitations, two central questions remain unanswered: what types of interactions ensure retrieval of target ordered structures, and what are the physical trade-offs of target retrieval in heterogeneous mixtures?

To answer these questions, we follow a novel approach: we prescribe a set of interactions and analytically derive the conditions under which these guarantee stability of target phases. Our choice of interactions is based on an analogy between the nucleation of target liquid phases and the retrieval of patterns in Hopfield neural networks [18], see also [3, 10]. We thus refer to this model as the liquid Hopfield model. For this model, we find conditions to ensure stability of up to $p = N - 1$ target phases, for arbitrary values of N and Q . One key condition is the presence of non-linear repulsive interactions, which stabilize retrieval. We further show that when such non-linearities are weak the mixture tends towards localized phases, in line with prior numerical evidence [11, 12], and show that perfect localization occurs at zero temperature. Overall, our work establishes that multi-component mixtures ex-

hibit a trade-off between localization and retrieval, with non-linearities playing a key role in leveraging this trade-off.

This paper is organized as follows. In section II we summarize the thermodynamics of multi-component liquid mixtures in the grand-canonical ensemble. Section III frames the problem of retrieval in liquid mixtures and defines the interaction matrix which completes the *liquid Hopfield model*. In sections IV-VII we study homogeneous, retrieval and localized states for a particular choice of targets, which we later show to be the worst-case scenario of the *liquid Hopfield model*. Section VIII extends our results to arbitrary targets. Lastly, in section IX we put summarise the results of this paper and put them in the context of current advances in multi-component mixtures.

II. THERMODYNAMICS OF HETEROGENEOUS FLUID MIXTURES

We consider a multi-component fluid mixture of N molecular species with densities ρ_i , where $i = 1, 2, \dots, N$. The thermodynamic behavior of this fluid is dictated by the free energy density

$$f(\{\rho_i\}, T) = u(\{\rho_i\}) - T s(\{\rho_i\}), \quad (1)$$

where u is the energy density, s is the entropy density [19], and T is the temperature; curly brackets denote the vector of all densities.

A generic form for the entropy density can be obtained by taking the mean-field limit of a microscopic lattice gas model, see e.g. Refs. [11, 20–22]. The resulting expression is

$$s(\{\rho_i\}) = -k_B \sum_{i=1}^N \rho_i \log(\rho_i) - k_B(1 - \rho) \log(1 - \rho), \quad (2)$$

where k_B is Boltzmann's constant (in what follows we set $k_B T = 1$) and $\rho = \sum_{i=1}^N \rho_i$ the total density. Nota bene, the entropy diverges for $\rho_i = 0$ or $\rho = 1$, which constrains the densities to the interior of the $N - 1$ dimensional standard simplex.

We characterize the internal energy via a low-density expansion and truncate to cubic order, instead of the common quadratic form [1, 11]. For simplicity, we take the cubic term to be diagonal, and so

$$u(\{\rho_i\}) = -\frac{v_2}{2} \sum_{i=1}^N \sum_{j=1}^N J_{ij} \rho_i \rho_j + \frac{v_3}{6} \sum_{i=1}^N \rho_i^3 N^2, \quad (3)$$

where $v_2 > 0$ and $v_3 > 0$ are constants that quantify the strength of the interactions and J_{ij} is the pairwise affinity matrix (the N^2 factor keeps the scale of the term proportional to v_3 independent of N for $\rho_i \sim N^{-1}$). Note that the quadratic term can be attractive ($J_{ij} > 0$) and repulsive ($J_{ij} < 0$), whereas we only consider a repulsive

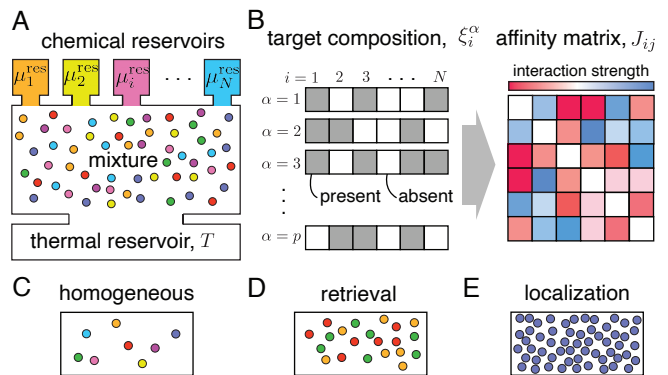


FIG. 1. *Schematic representation of setup.* **A.** A mixture with components $i = 1, \dots, N$ is in contact with a thermal reservoir at temperature T and chemical reservoirs with chemical potentials μ_i^{res} . **B.** Binary composition target vectors ξ_i^α indicate which components should be present in retrieval states of interest. The p targets are used to design the affinity matrix J_{ij} . Depending on the thermodynamic parameters, we distinguish three different regimes: **C.** The homogeneous regime, where all components mix equally; **D.** the retrieval regime, where the retrieval states are all simultaneously stable; **E.** and the disordered regime, where different states are stable including states with few components.

cubic term. The role of the cubic term will become clear later.

To study metastable states of this mixture, we consider a setting in which the fluid is in contact with a thermal reservoir at temperature T and N chemical reservoirs with chemical potentials μ_i^{res} , see Fig. 1A. Hereafter, we assume for simplicity that all chemical potentials are equal, i.e., $\mu_i^{\text{res}} = \mu^{\text{res}}$. Metastable states are determined by densities $\{\rho_{*,i}\}$ that satisfy the following two conditions.

The first condition is *chemical equilibrium*, by which the chemical potentials of the fluid, $\partial f / \partial \rho_i$, matches those of the reservoir, i.e.,

$$\frac{\partial f}{\partial \rho_i}(\{\rho_{*,j}\}) = \mu^{\text{res}}, \quad (4)$$

for all $i \in \{1, 2, \dots, N\}$.

The second condition is *mechanical stability*, i.e., the Hessian $H_{ij} = \partial^2 f / \partial \rho_i \partial \rho_j$ (inversely proportional to the isothermal compressibility [19]) is positive semi-definite,

$$\sum_{i=1}^N \sum_{j=1}^N H_{ij}^* x_i x_j \geq 0, \quad (5)$$

where $H_{ij}^* = H_{ij}(\{\rho_{*,k}\})$ and $\{x_i\}$ are arbitrary vectors. The equality in (5) is attained when $\{\rho_{*,i}\}$ is located at the *spinodal* manifold.

Defining the functional

$$\omega(\{\rho_i\}, \mu^{\text{res}}) = f(\{\rho_i\}) - \rho \mu^{\text{res}}, \quad (6)$$

which we call the *extended potential*, chemical equilibria are stationary points of ω w.r.t. $\{\rho_i\}$ at fixed μ^{res} . Such points are mechanically stable when they are *local minima* of the extended potential. The grand potential of the fluid mixture is given by the value of ω evaluated at its global minimum.

III. METASTABLE TARGETS AND RETRIEVAL

We use the framework of Sec. II to study the physical limitations on the metastability of states with specified compositions. To this aim, we construct an affinity matrix J_{ij} so that there exist p metastable states $\rho_{*,i}^\alpha$ with $\alpha = 1, \dots, p$, which we name *retrieval* states, corresponding to pre-defined *target* composition vectors ξ_i^α . The *targets* have binary entries that determine whether component i should be enriched ($\xi_i^\alpha = 1$) or depleted ($\xi_i^\alpha = 0$), see Fig. 1A and B. A fluid with such an affinity matrix J_{ij} is able to “retrieve” any retrieval state $\rho_{*,i}^\alpha$ by enhancing the density of some (but not all) of the components that are enriched in α . The remaining components, will be spontaneously retrieved by the mixture.

To endow the fluid with this retrieval capability, we draw inspiration from the classical work on neural networks by J.J. Hopfield [23] and propose as affinity matrix

$$J_{ij} = \sum_{\alpha,\beta=1}^p \gamma_i^{(\alpha)} c_{\alpha\beta}^{-1} \gamma_j^{(\beta)}, \quad (7)$$

where $\gamma_i^{(\alpha)} = (\xi_i^{(\alpha)} - q)/n$ are the shifted target composition vectors, $c_{\alpha\beta} = \sum_i \gamma_i^{(\alpha)} \gamma_i^{(\beta)}/N$ is a covariance matrix, and $c_{\alpha\beta}^{-1}$ its inverse. Here, $q = Q/N$ is the sparsity parameter, equal for all targets, with Q the number of components i enriched in the target compositions (i.e., for which $\xi_i^{(\alpha)} = 1$, see Fig. 1B), and $n = \sqrt{q(1-q)}$ a normalization factor. Due to its combination of concepts from multi-components fluids and neural networks, we refer to this model as the *liquid Hopfield model*. Notice that, in fact, for orthogonal $\gamma_i^{(\alpha)}$ we recover

$$J_{ij} = \sum_{\alpha=1}^p \gamma_i^{(\alpha)} \gamma_j^{(\alpha)}, \quad (8)$$

which we recognize as the interaction matrix used by Hopfield in Ref. [18].

In the following Secs. IV-VII, we consider the model in the special case of $q = 1/2$ and with $\gamma_i^{(\alpha)}$ the columns of Sylvester-Hadamard matrices (see Appendix A). This scenario, which we term the *hypersymmetric* case, is analytically solvable. While particular, we show in Appendix D that the hypersymmetric case is the most stringent one, i.e., when these targets are stable, then for the same parameter values ($v_2, v_3, \mu^{\text{res}}, p, N$, and Q) any other targets with binary compositions are also stable. In Sec. IX, we combine analytical and numerical approaches to study the general case of arbitrary binary targets.

IV. STATE STABILITY DIAGRAM

The main results of this Paper on the hypersymmetric case are contained in the state stability diagram of Fig. 2. This Figure depicts the region where the homogeneous state of the mixture is stable (violet), the region where all p retrieval states are stable and can be retrieved (green), and two additional regions where neither the homogeneous or retrieval states are stable (grey and orange). Boundaries of these regions are the *spinodal* lines of the corresponding states.

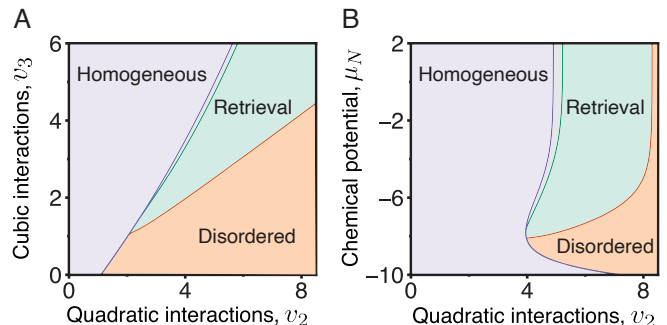


FIG. 2. *Stability diagrams for the homogeneous and retrieval states.* **A.** The spinodal lines (or stability boundaries) are obtained by solving the conditions of chemical and mechanical equilibrium (Eqs. (4-5)) analytically. The violet line corresponds to the boundary of the homogeneous regime and the green and orange lines to those of the retrieval regime. In the homogeneous regime, all components are present in equal amounts. In the retrieval regime, the p retrieval states, each enriched in Q components, are stable. Quadratic v_2 vs cubic v_3 interaction strength representation for $\mu_N = -6$. Notably, retrieval only occurs for strong enough cubic interactions, v_3 . **B.** Chemical potential μ_N vs quadratic interaction strength v_2 . The cubic interactions are held constant at $v_3 = 4$. The system needs to be held at high enough concentrations for retrieval to be stable.

The stability of the homogeneous state for $v_2 \approx 0$ is expected, as in this regime contributions from entropy and cubic repulsion dominate, which mix all different components equally.

The retrieval states are not stable in the commonly studied scenario when cubic repulsion is absent, i.e., $v_3 \approx 0$. Remarkably, for sufficiently large repulsion, retrieval of target compositions is possible and retrieval states are thus stable. The stability of retrieval states is separated from that of homogeneous states by a small transition region. The region with stable retrieval states expands as v_3 and v_2 increase.

For v_2 large enough, stability of retrieval states is lost and the system enters a disordered region in which many different non-retrieval states are locally stable. For $v_2 \gg v_3$, states with few components, which we call *localized* states, are globally stable. Since the cubic repulsive term penalizes such localized states, this elucidates the role of cubic repulsion in stabilizing retrieval states.

V. HOMOGENEOUS REGION

The homogeneous state of the mixture has component densities $\rho_i^{\text{hom}} = \rho/N$. In Appendix B, we show that homogeneous states satisfy the condition of chemical equilibrium, given by Eq. (4), when $\rho = \rho_*$ with

$$\rho_* = \frac{1}{1 + \exp(-\mu_N + \frac{v_3}{2}\rho_*^2)}, \quad (9)$$

and where

$$\mu_N = \mu^{\text{res}} + \ln N \quad (10)$$

is a rescaled chemical potential. Note that in the limit $N \gg 1$ for fixed μ^{res} , it holds that $\mu_N \gg 1$ and $\rho_* \rightarrow 1$, whereas for fixed μ_N we have that ρ_* is independent of N . In the following, we work on the second, arguably more physical, ensemble.

Now, we study the stability of the homogeneous state. Equation (5) holds if and only if all eigenvalues of the Hessian H_{ij} are non-negative. We therefore diagonalized H_{ij} at the homogeneous state, see Appendix C, which we carried out analytically for arbitrary targets $\{\gamma_i^\alpha\}$. The non-negativity of the smallest eigenvalue yields the inequality

$$\rho_*(v_2 - v_3\rho_*) \leq 1. \quad (11)$$

The equality in (11) is attained at the *spinodal* manifold, denoted by the violet lines in Fig. 2, for which the homogeneous state is marginally stable; in the low-temperature and dense limit, $v_2 \gg 1$ and $\mu_N \gg 1$, this reduces to $v_3 \sim v_2$. At the *spinodal* manifold, the unstable modes are spanned by the subspace of the target compositions γ_i^α . While this could be taken to suggest that the corresponding retrieval states ρ_{*i}^α are stable, see also analysis in [1, 13, 24, 25], we will later show that this is only the case in presence of cubic repulsion.

VI. RETRIEVAL REGION

In the retrieval region the mixture can adopt a stable density pattern according to a particular target α . In particular, the density of component i is enriched when $\gamma_i^{(\alpha)} = 1$ and depleted when $\gamma_i^{(\alpha)} = -1$. Therefore, to characterize retrieval we use the *ansatz*

$$\rho_i^\alpha = \frac{\rho}{N}(1 + a\gamma_i^{(\alpha)}) \quad (12)$$

for retrieval states, where $a \in [-1, 1]$ measures the degree of retrieval, and which we call the *overlap* between the state of the mixture and the target state [23]. Imposing chemical equilibrium on this *ansatz* results in the conditions

$$a_* = \tanh[a_*\rho_*(v_2 - v_3\rho_*)], \quad (13)$$

$$\rho_* = \frac{1}{1 + \exp(-\mu_N + \frac{v_3}{2}\rho_*^2(1 + a_*^2) + \frac{1}{2}\ln(1 - a_*^2))},$$

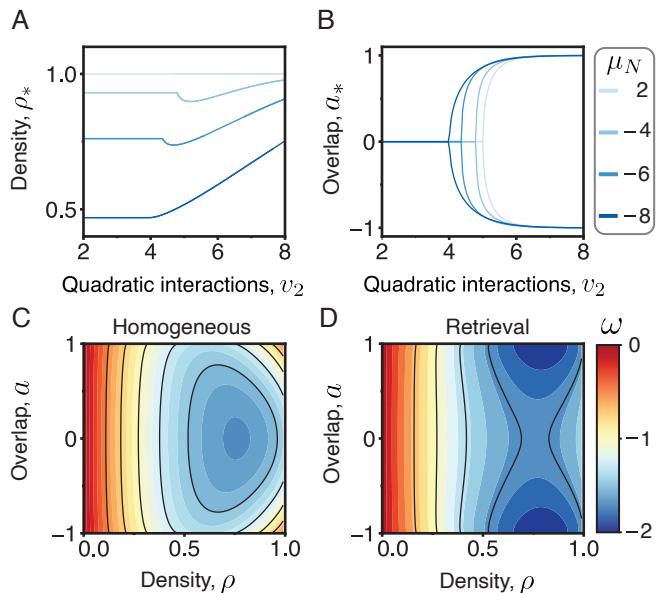


FIG. 3. *Stationary points of the homogeneous and retrieval states.* **A.** The overlap in chemical equilibrium, a_* vs quadratic interaction strength, v_2 is shown for different values of the chemical potential, μ_N . The overlap becomes non-zero outside the homogeneous region, indicating the emergence of the retrieval region. **B.** The total density in chemical equilibrium ρ_* is shown as a function of the strength of the quadratic interaction v_2 . The system becomes saturated for strong chemical potentials. **C.** Extended potential ω heatmap at $v_2 = 2$ and $\mu_N = -6$ in the (a, ρ) plane. The minima corresponds to the homogeneous phase. **D.** Extended potential ω heatmap at $v_2 = 6$ and $\mu_N = -6$ in the (a, ρ) plane. The symmetric minima that appears corresponds to a retrieval state ($a > 0$) and its mirror counterpart ($a < 0$). For both panels the cubic interaction is fixed at $v_3 = 4$.

see Appendix B for a detailed derivation.

In Fig. 3A and B, we plot the solutions of (13) as a function of the quadratic interaction strength, v_2 , for different values of the rescaled chemical potential, μ_N . The figure shows that the retrieval state emerges from the homogeneous state at the spinodal line. We remark that due to the $a_* \rightarrow -a_*$ symmetry in (13) (consequence of $q = 1/2$) a second state also emerges in which enrichment is opposite to that of the target α . Evaluating the potential $\omega(\{\rho_i\})$ in the subspace spanned by Eq. 12 suggests that the retrieval state is not only a stationary point, but a stable minimum, see Fig. 3C and D. However, a complete stability picture requires studying the N -dimensional stability condition in (5), which we do in the following.

In Appendix D, we derive an analytical expression for the smallest eigenvalue of the Hessian at chemically stable retrieval states. Depending on the set of targets there are two possible scenarios for the lowest eigenvalue of the Hessian. Here we consider the most stringent (and most common) scenario, while the other one is discussed a follow-up paper [26]. The retrieval state is stable when

the following two conditions hold

$$\rho_* (1 + a_*) (v_2 - v_3 \rho_* (1 + a_*)) \leq 1, \quad (14)$$

and

$$\rho_* (1 - a_*) (v_2 - v_3 \rho_* (1 - a_*)) \leq 1, \quad (15)$$

where (ρ_*, a_*) are taken from (13). The two equalities in the above equations correspond to the orange and green lines, respectively, of Fig. 2 when $a_* > 0$ (and the other way around when $a_* < 0$). The corresponding instability modes are confined into the space spanned by the target compositions. The existence of two conditions reflects the fact that retrieval is bounded by homogeneous states, for low v_2 , and disordered states, for high v_2 . Note however that between the homogeneous and retrieval regions there exists a narrow transition band. In the low-temperature and high density regime the width of the transition region scales as $\sim \log(v_2)$, while the width of the retrieval region scales as $\sim v_2/2$.

Two important facts can be deduced from (14). First, in absence of the repulsive cubic interaction, i.e. $v_3 = 0$, adding the inequalities gives $\rho_* v_2 \leq 1$, which by Eq. 12 implies that $a_* = 0$, and so there are no retrieval states, see also Fig. 2. Therefore, sufficiently strong non-linear repulsion is necessary for retrieval. Second, Eq. (14) does not depend on the number of species N nor on the number of targets p . Consequently, the symmetric liquid Hopfield model allows up to $N - 1$ target compositions to be simultaneously stable, provided cubic repulsion is strong enough.

While stability of retrieval states is independent on the number of components N and targets p , the sizes of the basins of attraction do depend on p and N . To investigate this point, we study the gradient descent dynamics on the potential landscape ω at fixed chemical potentials near a retrieval state $\rho_{*,i}^\alpha$. We initiate gradient descent in states ρ_i that are equal to $\rho_{*,i}^\alpha$ in $1 - r$ components and equal to ρ_*/N in the remaining r components. We quantify the size of the basin of attraction as the minimal value of r for which the gradient descent dynamics converges to the retrieval state $\rho_{*,i}^\alpha$. Figure 4A shows how the size of the basin of a given target, $1 - r$, depends on the number of targets, p , for mixtures with different number of components, N . Basins decrease in size as p increases, as expected, and so retrieval is effectively more difficult as more targets are encoded. We therefore conclude that the mid-point of this decrease, $p_{1/2}$, measures the capacity of a liquid mixture to encode different target compositions. Interestingly, we find that this mid-point increases linearly with the number of components, N , see Figure 4B. This implies that as the number of components in a mixture increases, the number of retrieval states that can be retrieved also increases. This scaling is reminiscent of the behavior of the capacity of associative neural networks [23].

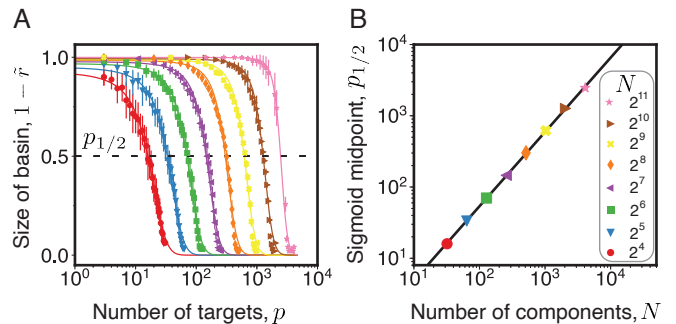


FIG. 4. *Scaling of basins of attraction* **A**. Size of the basin of attraction of retrieval states, $1 - \tilde{r}$ vs number of targets, p for different number of components, N . Each point corresponds to an average of 20 independent choices of the set of targets and the retrieval state. In addition, the retrieval state is perturbed with a fraction r of the densities set to those of the homogeneous state. We consider 50 cases of such perturbations with r ranging from 0, 1. The value \tilde{r} is defined as the value of r at which the success rate of gradient descent minimization is equal to the threshold 0.99. Sigmoidal curves are fit to each set of points. As the number of targets increases, the size of the basin of attraction shrinks. **B**. Scaling of the mid-point of each sigmoidal, $p_{1/2}$, as a function of the number of components, N . A line is fitted to the points showing that a linear scaling is compatible, yielding $p_{1/2} = 0.720N - 15.5$, with relative uncertainties of both coefficients ($2.3 \cdot 10^{-3}$, 3.8). Other parameters are fixed, for both plots, to $\mu_N = 1$, $v_2 = 6$ and $v_3 = 4$.

VII. LOCALIZATION IN THE DISORDERED REGION

We now focus on the disordered region, where neither the homogeneous nor the retrieval states are stable. One of the key features of this region is that locally stable states overlap with multiple target compositions, yet they are enriched in a small fraction of components.

We first consider the analytically solvable case of $v_3 = 0$, $\mu = 0$, and $v_2 \gg 1$. In this case, the extended potential ω takes the quadratic form

$$\omega(\{\rho_i\}) = -\frac{v_2}{2} \sum_{i,j=1}^N J_{ij} \rho_i \rho_j. \quad (16)$$

Minimising a quadratic function over a simplex is an NP-hard problem called the quadratic concave optimization problem, see Refs. [27–29]. However, for the specific choice of J_{ij} in Eq. (7) it holds that

$$\omega(\{\rho_i\}) = -\frac{v_2}{2} \rho^2 \sum_{\alpha=1}^p m_\alpha^2, \quad (17)$$

where $m_\alpha = \sum_{i=1}^N \gamma_i^{(\alpha)} \rho_i$. As $|m_\alpha| \leq 1$, the states that minimize ω must satisfy $\rho = 1$ and $m_\alpha = \pm 1$ for all values of α . States in which only one component is enriched, i.e. $\rho_i^{(k)} = \delta_{i,k}$ with $k \in \{1, 2, \dots, N\}$ fixed, are instances

of such minima located at the corners of the simplex. Furthermore, for large enough values of p these states are the only configurations that minimise ω as a probabilistic argument in Appendix F shows.

Corners of the simplex are fully localised states in the set of components, in the sense that they are enriched in only one component. This is reminiscent of Anderson localisation for electrons in disordered materials [30, 31]. More generally, we say that a state $\{\rho_i\}$ is *localised* when the number of nonzero entries stays finite in the limit $N \gg 1$. For finite N , localization is quantified by the *participation ratio*

$$\text{PR}(\{\rho_i\}) = \frac{1}{N} \frac{\left(\sum_{i=1}^N \rho_i\right)^2}{\sum_{i=1}^N \rho_i^2}, \quad (18)$$

with $\lim_{N \rightarrow \infty} \text{PR}(\{\rho_i\}) > 0$ for a delocalised state, and $\lim_{N \rightarrow \infty} \text{PR}(\{\rho_i\}) = 0$ for a localised state. In what follows, we characterize local minima in the disordered region using the participation ratio.

Figure 5 summarizes results of minimizing the extended potential numerically. Panel A shows the participation ratio of minima of ω as a function of v_2 . For low v_2 the homogeneous state is stable, and so $\text{PR} = 1$. At intermediate v_2 the retrieval state becomes stable, for which $\text{PR} = 1/(1 + a_*^2)$. In addition we also observe other non-retrieval states that are locally stable, which are reminiscent of spurious states in associative neural networks [23?]. For large values of v_2 , these non-retrieval states have a decreasing PR, with the discrete jumps observed corresponding to the full depletion of components one by one. Furthermore, Fig. 5B shows that as v_3 decreases the global minimum lowers its PR and the retrieval region shrinks.

We now study the role of increasing the number of components on stable states of the disordered region. Fig. 5C shows that the PR decreases as a function of N for fixed v_2 . Moreover, Fig. 5E shows that the PR saturates to a constant value as N increases. This asymptotic value decreases as a function of the quadratic interaction, v_2 , and the number of targets, p , see Fig. 5D. Therefore stable states are localized for $v_2 \gg 1$ and an extensive number of targets $p \sim N$, in agreement with the analytical results at the beginning of this section.

Taken together, stable states in the disordered region have a small PR and localize in the limit of v_2 large and many targets $p \sim N$. This supports the idea that stability of the retrieval region is related to the suppression of localization.

VIII. GENERALIZATION TO ANY TYPE OF TARGETS

Up until now, we have restricted our study to the symmetric case described at the end of section III. We now generalize our results to non-orthogonal targets with arbitrary sparsity q . In this general setting, retrieval states

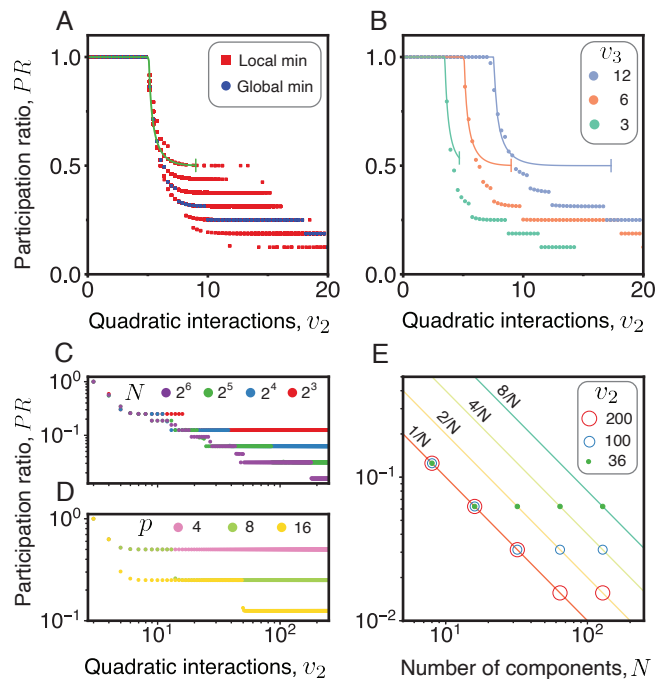


FIG. 5. *Non-retrieval and localization.* Points shown are the result of numerically minimizing the extended potential $\omega(\{\rho_i\})$ at fixed $\mu_N = 1$. **A.** Participation ratio, PR vs quadratic interaction strength, v_2 for $v_3 = 6$. The green line indicates the participation ratio of the homogeneous and retrieval states. There are several minima which are not homogeneous nor retrieval states. **B.** Participation ratio of the global minima, PR vs quadratic interactions, v_2 for different values of the cubic interactions, v_3 . The lines plotted correspond to the homogeneous and retrieval states. As v_3 increases the global minima has lower PR and is enriched in fewer components. Parameters used for both panels: $p = 17, N = 32$. **C.** Participation ratio of the global minimum vs quadratic interaction strength, v_2 for different number of components, N . The minima found for strong v_2 is enriched in fewer components the larger N is. Parameters used: $p = 24, v_3 = 3$. **D.** Participation ratio of the global minimum vs quadratic interactions, v_2 for different number of targets p . As the number of targets increases the minima is enriched in fewer components. Parameters used: $N = 32, v_3 = 3$. **E.** Participation ratio of the global minimum vs number of components N for increasing values of the quadratic interaction, v_2 . The minima is localized for strong enough v_2 . Parameters used: $p = 24, v_3 = 3$.

$\{\rho_i^\alpha\}$ can also be in chemical equilibrium. The conditions on ρ_* and a_* are derived in Appendix B and generalize those in Eq. (13).

Figure 6A shows the stability diagram for a small number of non-orthogonal targets with $q = 1/2$. Unlike the symmetric case in Fig. 2, for non-orthogonal targets each retrieval state has a distinctive *spinodal* line. This results in a region of parameters for which only some of the retrieval states are stable, which we term *quasi-retrieval*. In addition, a retrieval region, in which all targets are simultaneously stable, is also present. In Appendix D we show

that this retrieval region is bounded from above by the *spinodal* of the symmetric case, Eq. (14). Interestingly, Fig. 6B reveals that as the number of targets increases the quasi-retrieval region gradually decreases in size until it coincides with the *spinodal* line of the symmetric case. This can be understood from the properties of the Hessian (see Appendix D). We conclude that the symmetric case determines the region of stability of retrieval states with non-orthogonal targets for large p , and bounds it for small p . Therefore, while seemingly specific, the symmetric case constitutes the most stringent scenario.

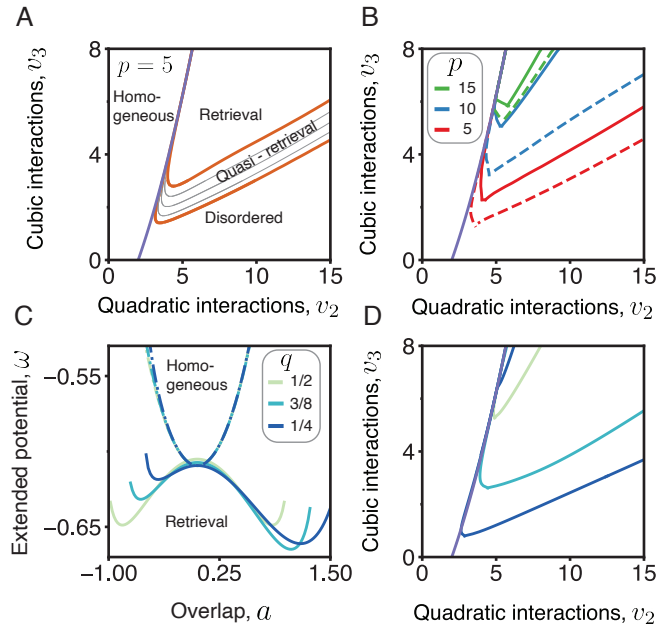


FIG. 6. *Retrieval of arbitrary targets* **A**. Stability diagram in the interaction strength plane, v_2 vs v_3 , for $p = 5$. Notice the appearance of the regime of quasi-retrieval shown in a dashed line. Here only some targets are retrieved, the stability lines of which are shown in grey. **B**. Stability diagram in the interaction strength plane, v_2 vs v_3 , for different number of targets. The lines corresponds to an average of 10 independent sets of targets. As the number of targets increase the quasi-retrieval and retrieval region shrink. **C**. The parameterized extended potential $\omega(a, \rho)$ evaluated at ρ_* , $v_3 = 4$ as a function of the overlap a for varying values of the sparsity q . The single-well potential corresponds to the homogeneous regime $v_2 = 2$ and the double-well potential to the retrieval $v_2 = 8.5$. Notice the break of symmetry for $a \rightarrow -a$. **D**. Phase stability diagram for different values of the sparsity for $p = 25$. Parameters used $N = 32, \mu_N = 0$.

So far we have focused on the case of $q = 1/2$ in which targets are enriched in half of the components of the mixture. This is a very restrictive scenario, and so we now generalize to the case in which the sparsity parameter is lower, $q < 1/2$, and so targets may contain only a small fraction of the components in the mixture. Changing the sparsity of the targets from $q = 1/2$ breaks the symmetry $a \rightarrow -a$ between target and anti-target. This can be

seen in Fig. 6C, where the asymmetry in the extended potential ω as a function of a is apparent. Consequently, the case of low q suppresses anti-targets. Furthermore, as shown in Fig. 6D increasing the sparsity of targets, i.e. reducing q , results in a larger retrieval region. Interestingly, we find that in the limit $q \rightarrow 0$ targets still require a finite amount of cubic repulsion, i.e. $v_3 \neq 0$, see Appendix G. This highlights the role of non-linearities, which can only be as small as the quadratic interaction dictates.

IX. DISCUSSION

Biological liquid mixtures often consists of a large number of different components [8, 32–35]. Despite this, such mixtures are not disordered, but instead assemble into functional states with well characterized composition. Resolving this apparent paradox is challenging because at present there is no established approach to describe materials with a large number of components.

In this paper we have introduced the liquid Hopfield model as a simple paradigm for multi-component mixtures capable of retrieving multiple target compositions, see Fig. 1. In it, we combined a classical statistical physics liquid model with interactions among components inspired by Hopfield neural networks. Our model reveals a trade-off between target retrieval states and localized states, in which only few components are enriched. Stability of retrieval states is achieved by suppressing localization through repulsive non-linear interactions. The role of this non-linearity, which can be interpreted as a higher order term in the virial expansion of the free energy, becomes less important as targets themselves become localized. Taken together, this sheds light on the relation between localisation, as observed in previous works [11, 12, 17], and the retrieval capacity of complex liquids.

The liquid Hopfield model is part of a family of Sear-Cuesta-like models for multicomponent mixtures that rely on free energies of the form (1-3)) with large values of N , see e.g. [1, 13, 15, 25]. However, previous studies were limited to the study of the instabilities of the high temperature homogeneous state [1, 13, 25]. In contrast, in the present work we have analytically characterised ordered states that are stable. These retrieval states appear at low temperatures when the homogeneous state is unstable and are an example of the emergence of order in a heterogeneous liquids.

Lowering the temperature even further, the retrieval states get unstable and the liquid Hopfield model exhibits a disordered region. The disordered region is a generic feature of multicomponent mixtures described by free energies of the form (1-3), see [1, 11, 12]. It is difficult to fully characterise the disordered region as finding the minimal configurations of the free energy (1-3) at zero temperature is equivalent to the quadratic programming problem, which is NP-hard [27–29], and consequently,

the low temperature region has a rugged landscape, akin to the low-temperature phase of spin glasses [36, 37]. In spite of this complication, numerical results in this paper show that states in the low-temperature region tend to localise, consistent with results from previous works [11, 12], and these localised states dominate the natent version of the liquid Hopfield model without repulsive, cubic interaction term.

To make the liquid Hopfield model work, we require a nonlinear interaction term that counters for the tendency at low temperatures of states to localise. The necessity of nonlinear interaction term is consistent with results from neural network theory. Indeed, although the Hopfield model has mostly been studied for discrete variables [18, 23, 38], there do exist a few studies on Hopfield models with continuous variables defined on either a sphere [39] or in \mathbb{R}^N [40, 41]. These models are analytically more tractable than the liquid Hopfield model as the phase space does not have the complicated boundary of an $N - 1$ -dimensional simplex. In both models, a quartic term in the potential is necessary for successful retrieval. It should be noted that even though the free energy functional (1-3) has nonlinear entropic terms, the present paper's results show that these entropic terms are not nonlinear enough to guarantee retrieval. In fact, in a follow up paper we show that a cubic, or higher order, repulsion term is necessary to observe retrieval [26]. For the above reasons, we do expect that the requirement of a nonlinear term in the liquid Hopfield model is a generic feature and not an artefact of the model we have studied.

Note that the nonlinear term was not necessary in Ref. [17] that builds liquid models with a set of stable target states through numerical optimisation. However, a closer inspection of the results in Ref. [17] made us conclude that [17] focuses on the regime $Q \approx 0$, and hence the results obtained are consistent with the findings in the present paper.

The interaction terms used in the liquid Hopfield model are closely related those of models for *multifarious* self-assembly of solid structures [3, 10]. The main difference between the liquid Hopfield model and these physical models is that the former uses the physics of liquids, as described by Eqs. (1-3)), while the latter rely on models defined on lattices that are solved with simulations. Nevertheless, it would be interesting to relate the results obtained in liquids with those for the self-assembly of solid structures.

Our research opens many natural avenues of future research, of which we just highlight three key aspects. First, our study has focused on the grand-canonical ensemble, which leaves open extending our results and analytical approach to the canonical ensemble. Second, our model is purely equilibrium, which leaves open the role of dissipation, e.g. in stabilizing target phases. Third, while we assumed a particular set of interactions, we have not addressed how such interactions can be achieved. Clearly, protein affinities are not random, but have instead evolved to comply with a particular function [16].

It thus remains open whether evolutionary dynamics can parsimoniously converge to the affinity matrix we considered, recapitulating the success of neuronal learning rules. Overall, we consider our work as an important step in establishing an analytical framework in the study of multi-component mixtures, a vibrant emerging field in soft and hard condensed matter physics.

ACKNOWLEDGMENTS

Acknowledge the cluster people at Gulbenkian. GC is supported by the EPSRC Centre for Doctoral Training in Cross-Disciplinary Approaches to Non-Equilibrium Systems (CANES, EP/L015854/1). RBT acknowledges financial support from the Portuguese Foundation for Science and Technology (FCT) under the contract 2022.12272.BD.

Appendix A: Targets in the symmetric case

We now specify the ensemble of targets $\gamma_i^{(\alpha)}$ in the symmetric case of our model. To do so, we first introduce the Sylvester-Hadamard matrices of order $M = 2^k$, $\mathcal{H}(k)$ [42]. These matrices are constructed starting from the matrix $\mathcal{H}(1)$ using the following iterative approach:

$$\mathcal{H}(1) = \begin{bmatrix} 1 & 1 \\ 1 & -1 \end{bmatrix} \Rightarrow \mathcal{H}(k) = \begin{bmatrix} \mathcal{H}(k-1) & \mathcal{H}(k-1) \\ \mathcal{H}(k-1) & -\mathcal{H}(k-1) \end{bmatrix}, \quad (\text{A1})$$

which results in the first column having all components equal to one. Hereafter we do not explicitly indicate the size k of the matrices.

Importantly, the columns of these matrices form a boolean group. In particular, for any two columns u and v with elements $\{\mathcal{H}_{iu}\}$ and $\{\mathcal{H}_{iv}\}$, there exists a third column w such that

$$\mathcal{H}_{iw} = \mathcal{H}_{iu}\mathcal{H}_{iv}. \quad (\text{A2})$$

This follows from the fact that the columns of \mathcal{H} can be expressed as

$$\mathcal{H}_{iu} = (-1)^{\sum_{\ell=1}^k n_{\ell}^{(i)} n_{\ell}^{(u)}}, \quad (\text{A3})$$

where the $n_{\ell}^{(i)}$ are the digits of i when it is written in the base-2 numeral system, i.e., $i = \sum_{\ell=1}^k n_{\ell}^{(i)} 2^{\ell-1}$.

We can now characterize the targets for the symmetric liquid Hopfield model. For $p = M - 1$, the targets correspond to columns of Sylvester-Hadamard matrices, i.e. $\gamma_i^{(\alpha)} = \mathcal{H}_{iu}$, excluding the first column $u = 1$. For $p < M - 1$, the targets are chosen at random among columns $u > 1$ of Sylvester-Hadamard matrices ensuring that for each target state $\gamma_i^{(\alpha)}$ there exists two target states $\gamma_i^{(\beta_1)}$ and $\gamma_i^{(\beta_2)}$ such that (A2) is satisfied, that is:

$$\gamma_i^{(\alpha)} = \gamma_i^{(\beta_1)} \gamma_i^{(\beta_2)}. \quad (\text{A4})$$

For $p > M/2$, the latter condition is satisfied for all combinations of p targets. Indeed, this can be proven through contradiction. Assume that there exists one target state, say $\gamma_i^{(\alpha)}$, for which there exist no two other target states $\gamma_i^{(\beta_1)}$ and $\gamma_i^{(\beta_2)}$ such that (A4) holds. In this case, we can construct the $p-1$ vectors $\zeta_i^{(\beta)} = \gamma_i^{(\alpha)} \gamma_i^{(\beta)}$ with $\beta \neq \alpha$, which by assumption are not target states. However, since the columns of the Hadamard matrix form a group under the element wise product, the $\{\zeta_i^{(\beta)}\}$, with $\beta \neq \alpha$, are $p-1$ distinct columns of the Hadamard matrix. Hence, within our assumptions, the $p-1$ vectors $\{\zeta_i^{(\beta)}\}$ with $\beta \neq \alpha$, the $p-1$ target states $\{\gamma_i^{(\beta)}\}$ with $\beta \neq \alpha$, the target state $\{\gamma_i^{(\alpha)}\}$, and the all-ones vector, should all be distinct columns of the Hadamard matrix. However, this is not possible as we count $2p > M$ vectors and the Hadamard matrix has by construction only M columns.

Appendix B: Chemical equilibrium for homogeneous and retrieval states

In this appendix we derive the conditions under which the *ansatz* in Eq. (12) is in chemical equilibrium. We derive these conditions for the affinity matrices of the form in Eq. (7), which reduce to Eq. (13) for $q = 1/2$.

The condition for chemical equilibrium in Eq. (4) can be written explicitly as

$$-v_2 \sum_{j=1}^N J_{ij} \rho_j + \frac{v_3}{2} \rho_i^2 N^2 + \log \rho_i = \log(1-\rho) + \mu^{\text{res}}, \quad (\text{B1})$$

which yields N equations. Substituting the retrieval *ansatz* given by Eq. (12) into (B1) gives

$$\begin{aligned} & -v_2 \sum_{j=1}^N J_{ij} \frac{\rho}{N} (1 + a\gamma_j^{(\alpha)}) + \frac{v_3}{2} \rho^2 (1 + a\gamma_i^{(\alpha)})^2 \quad (\text{B2}) \\ & + \log \frac{\rho(1 + a\gamma_i^{(\alpha)})}{N} = \log(1-\rho) + \mu^{\text{res}}. \end{aligned}$$

We now use two properties of the affinity matrix J_{ij} of Eq. (7): first, the all-ones vector belongs to the kernel of J_{ij} ; and second, the target vectors, $\{\gamma_i^{(\alpha)}\}$, are eigenvectors of J_{ij} with eigenvalue N . From this, we can simplify Eq. (B2) into

$$\begin{aligned} & -v_2 \rho a \gamma_i^{(\alpha)} + \frac{v_3}{2} \rho^2 (1 + a\gamma_i^{(\alpha)})^2 + \log \frac{\rho(1 + a\gamma_i^{(\alpha)})}{N} \\ & = \log(1-\rho) + \mu^{\text{res}}. \end{aligned} \quad (\text{B3})$$

Note that because the targets are binary, this reduces the N stability equations to two equations: one for $\gamma_i^{(\alpha)} = (1-q)/n$ and the other for $\gamma_i^{(\alpha)} = -q/n$. Solving

these towards a and ρ we get the chemical equilibrium conditions for target states with arbitrary q :

$$a_* = n \frac{\exp(w) - 1}{1 - q + q \exp(w)}, \quad (\text{B4})$$

$$\begin{aligned} \frac{1}{\rho_*} &= 1 + \exp \left[-\mu_N + \frac{1}{2} v_3 \rho_*^2 (1 + a_*^2) \right. \\ & \left. + q \log \left(1 + a_* \frac{1-q}{n} \right) + (1-q) \log \left(1 - a_* \frac{q}{n} \right) \right], \end{aligned} \quad (\text{B5})$$

where $w = \frac{1}{n} [v_2 \rho_* a_* - \frac{1}{2} v_3 \rho_*^2 (2a_* + a_*^2 \frac{1-2q}{n})]$ and $n = \sqrt{q(1-q)}$. These equations reduce to Eq. (13) for $q = 1/2$. The value of ρ_* for the homogeneous state in Eq. (9) is the particular case of $a_* = 0$.

Appendix C: Exact diagonalization of the Hessian in homogeneous state

In this appendix we derive the conditions for mechanical equilibrium at the chemically stable homogeneous state determined by Eq. (9). To this end, we diagonalize the Hessian in a homogeneous state $\rho_i = \rho$, which takes the form

$$H_{ij} = -v_2 J_{ij} + \frac{1}{1-\rho} + \delta_{ij} \left(\frac{N}{\rho_i} + v_3 N \rho \right), \quad (\text{C1})$$

where J_{ij} is given by Eq. 7.

The spectrum of this matrix consists of three eigenvalues, which we denote by λ_{ret} , λ_{cond} and λ_{\perp} . The retrieval eigenvalue is

$$\lambda_{\text{ret}} = \frac{N}{\rho} + v_3 N \rho - v_2 N. \quad (\text{C2})$$

Its eigenspace is a p -dimensional vector space spanned by the p targets $\{\gamma_i^{(\alpha)}\}$ to be retrieved. The condensation eigenvalue is

$$\lambda_{\text{cond}} = \frac{N}{\rho} + v_3 N \rho + \frac{N}{1-\rho}, \quad (\text{C3})$$

and its corresponding eigenvector is the all-ones vector. The remaining eigenvalue is

$$\lambda_{\perp} = \frac{N}{\rho} + v_3 N \rho, \quad (\text{C4})$$

and has a $N - p - 1$ dimensional eigenspace that is orthogonal to the targets and the all-ones vector.

Since only λ_{ret} can be negative, the homogeneous state destabilises in a direction that is a linear combination of the target vectors. The condition in Eq. (11) is obtained by setting $\rho = \rho_*$ in the equation $\lambda_{\text{ret}} = 0$.

Appendix D: Lower bounds for eigenvalues of the Hessian in the retrieval state

Unlike in the homogeneous case, discussed in appendix C, we have not obtained an explicit expression

for the spectrum of the hessian in retrieval states. Nevertheless, we now derive a lower bound for the eigenvalues of the Hessian which provide sufficient conditions for retrieval. Furthermore, we also show that for the symmetric case described in A these conditions are in fact also necessary, which proves Eq. 14.

Substituting the retrieval ansatz (12) into the Hessian, $H_{ij} = \partial^2 f / \partial \rho_i \partial \rho_j$, we get the matrix

$$H_{ij} = -v_2 J_{ij} + \frac{1}{1-\rho} + N \delta_{i,j} \left[v_3 \rho (1 + a \gamma_i^{(\alpha)}) + \frac{1}{\rho} \frac{1}{1 + a \gamma_i^{(\alpha)}} \right]. \quad (\text{D1})$$

Substituting $\gamma_i^{(\alpha)} = (\xi_i^{(\alpha)} - q)/n$, and using that $\xi_i^{(\alpha)} \in \{0, 1\}$, we get

$$H_{ij} = -v_2 J_{ij} + \frac{1}{1-\rho} + N \delta_{i,j} \left(c_1 - c_2 \xi_i^{(\alpha)} \right), \quad (\text{D2})$$

where

$$c_1 = v_3 \rho (1 - aq/n) + \frac{1}{\rho} \frac{1}{1 - aq/n}, \quad (\text{D3})$$

and

$$c_2 = -\frac{v_3 \rho a}{n} + \frac{a}{n \rho (1 + a(1-q)/n) (1 - aq/n)}. \quad (\text{D4})$$

Since the matrix H_{ij} is symmetric, its minimal eigenvalue $\lambda_{\min}^{(\alpha)}$ can be obtained by solving the constrained minimization problem

$$\lambda_{\min}^{(\alpha)} = \min_{\|\{x_i\}\|=1} \left(\sum_{i=1}^N \sum_{j=1}^N x_i H_{ij} x_j \right), \quad (\text{D5})$$

where

$$\begin{aligned} & \sum_{i=1}^N \sum_{j=1}^N x_i H_{ij} x_j \\ &= -v_2 \sum_{i=1}^N \sum_{j=1}^N x_i J_{ij} x_j + \frac{1}{1-\rho} \left(\sum_{i=1}^N x_i \right)^2 \\ & \quad + N c_1 \sum_{i=1}^N x_i^2 - N c_2 \sum_{i=1}^N x_i^2 \xi_i^{(\alpha)}. \end{aligned} \quad (\text{D6})$$

Next, we bound $\lambda_{\min}^{(\alpha)}$ from below by bounding the four terms in Eq. (D6):

- *interaction* term: since the affinity matrix J_{ij} in Eq. 7 has two eigenvalues, namely 0 and N , it holds that

$$-v_2 \sum_{i=1}^N \sum_{j=1}^N J_{ij} x_i x_j \geq -v_2 N \sum_{i=1}^N x_i^2 = -v_2 N. \quad (\text{D7})$$

- *entropic* term: this term is non-negative, and so

$$\frac{1}{1-\rho} \left(\sum_{i=1}^N x_i \right)^2 \geq 0. \quad (\text{D8})$$

- c_1 -term: as the norm of $\{x_i\}$ equals one, this term is constant,

$$N c_1 \sum_{i=1}^N x_i^2 = N c_1. \quad (\text{D9})$$

- c_2 -term: depending on the sign of c_2 we get different bounds. If $c_2 > 0$, then

$$-N c_2 \sum_{i=1}^N x_i^2 \xi_i^{(\alpha)} \geq -N c_2. \quad (\text{D10})$$

On the other hand, if $c_2 < 0$, then

$$-N c_2 \sum_{i=1}^N x_i^2 \xi_i^{(\alpha)} \geq 0. \quad (\text{D11})$$

Adding the lower bounds for the individual terms, we get for $c_2 > 0$ that

$$\frac{\lambda_{\min}^{(\alpha)}}{N} \geq -v_2 + c_1 - c_2, \quad (\text{D12})$$

and for $c_2 < 0$,

$$\frac{\lambda_{\min}^{(\alpha)}}{N} \geq -v_2 + c_1. \quad (\text{D13})$$

The inequalities above can be used to derive sufficient conditions for retrieval, that is conditions on the parameters $\{v_2, v_3, \mu, q\}$ that, when satisfied, ensure stability of the retrieval states (but there may be other regions of parameters where retrieval is also stable). To do so, we set $a = a_*$ and $\rho = \rho_*$ from Eq. (B3), which ensures chemical stability, and then impose that the right-hand-side (RHS) of Eqs. (D12) and (D13) are greater or equal than zero. Since positivity of the RHS ensures $\lambda_{\min}^{(\alpha)} \geq 0$ we find the following sufficient conditions for stability of retrieval states, viz.,

$$-v_2 + c_1 - c_2 \geq 0 \quad (\text{D14})$$

for $c_2 > 0$, and

$$-v_2 + c_1 \geq 0 \quad (\text{D15})$$

for $c_2 < 0$. Note that if $c_2 > 0$, then (D14) implies (D15), and if $c_2 < 0$, then (D15) implies (D14). Hence, we can state mechanical stability conditions more simply as the requirement that both (D14) and (D15) are satisfied, without reference to c_2 . Remarkably, these (D14) and (D15) for retrieval do not depend on p . Eqs. D14 and

D15 were used in Fig. 6D to outline the boundary of the retrieval phase with arbitrary sparsity.

For the symmetric case described in Appendix A the inequalities in Eq. D12 and D13 saturate. This implies that the conditions in Eqs. D14 and D15 (evaluated for $q = 1/2$ and $n = 2$) are the necessary and sufficient conditions for stability of the retrieval state in the symmetric case, which correspond to Eqs. 14 and 14. To show the saturation of Eq. D12 in the symmetric case with $c_2 > 0$ we evaluate the quadratic function in Eq. D6 at

$$x_i = \frac{1}{\sqrt{2N}} \left(\gamma_i^{(\beta_1)} + \gamma_i^{(\beta_2)} \right). \quad (\text{D16})$$

Using the property Eq. A4 that holds in the symmetric case, we find that this choice of x_i saturates Eq. D12. For $c_2 < 0$ we obtain saturation using the vector

$$x_i = \frac{1}{\sqrt{2N}} \left(\gamma_i^{(\beta_1)} - \gamma_i^{(\beta_2)} \right). \quad (\text{D17})$$

Appendix E: Collapse of the retrieval lines in the limit of large p and $q = 1/2$

Asides from the symmetric case, the inequalities in Eqs. D12 and D13 saturate in the limit of a large number of targets p . While we observed this numerically for all values of q , below we provide an analytical derivation for the case $q = 1/2$, which explains why in Fig. 6B the spinodal lines are determined by the equalities in Eq. (14) for large p .

To prove the saturation, we note that the saturation of the inequalities (D14) and (D15) for (D16) and (D17) rely on the fact that (i) $\{x_i\}$ is an eigenvector of J_{ij} ; (ii) it is the linear combination of two vectors $\{\gamma_i^{(\beta_1)}\}$ and $\{\gamma_i^{(\beta_2)}\}$ for which it holds that $\gamma_i^{(\beta_1)}\gamma_i^{(\beta_2)} = \gamma_i^{(\alpha)}$.

Here, we follow a similar approach. We evaluate the quadratic form in Eq. D6 for the vector

$$x_i^{(+,\alpha)} = \frac{1}{\sqrt{2N}} \left(\zeta_i^{(\beta_1)} + \zeta_i^{(\beta_2)} \right) \quad (\text{E1})$$

where $\{\zeta_i^{(\beta_1)}\}$ and $\{\zeta_i^{(\beta_2)}\}$ are two vectors, not necessarily target states, with entries $\zeta_i^{(\beta_1)}, \zeta_i^{(\beta_2)} \in \{-1, 1\}$, for which $\sum_i \zeta_i^{(\beta_1)} = \sum_i \zeta_i^{(\beta_2)} = 0$, and with $\zeta_i^{(\beta_1)}\zeta_i^{(\beta_2)} = \gamma_i^{(\alpha)}$. Such two states can be constructed as follows. First, we select a state $\{\zeta_i^{(\beta_1)}\}$ with binary entries that is orthogonal to $\{\gamma_i^{(\alpha)}\}$ and to the all ones vector. Second, we define $\zeta_i^{(\beta_2)} = \zeta_i^{(\beta_1)}\gamma_i^{(\alpha)}$. Since $p = N - 1$, the affinity matrix $J_{ij} = \delta_{i,j} - 1$, $\{x_i^{(+,\alpha)}\}$ is an eigenvector of J_{ij} , and therefore the inequality (D14) is saturated for $\{x_i^{(+,\alpha)}\}$. Analogously, we can consider a vector $\{x_i^{(-,\alpha)}\}$ to obtain the second spinodal line (D15).

Appendix F: Equilibrium states at zero temperature

We now use a probabilistic argument to show that for $p > \log(N)/\log(2)$ the minima of the functional in Eq. (17) are the corners of the simplex of physical states. First, note that minima must have $\rho = 1$ and $m_\alpha = \pm 1$. Hence, minima are obtained as solutions to equations of the form $m_\alpha = \sigma_\alpha$, with $\alpha \in \{1, 2, \dots, p\}$ and $\sigma_\alpha \in \{-1, 1\}$. The values of σ_α determine the corner on which we focus. We discuss the case of $\sigma_\alpha = 1$ for all α , but the other cases can be treated equivalently. The effect of each equation is to set $\rho_i^\alpha = 0$ whenever $\gamma_i^\alpha \neq 1$. In this way, given a set of p targets, a noncorner solution exists whenever there exist two or more components, say i and j , for which it holds that $\gamma_i^\alpha = \gamma_j^\alpha = 1$ for all $\alpha \in \{1, 2, \dots, p\}$. That is, whenever two or more components are shared by all targets.

If the p targets are randomly selected, the probability that at least two components are shared in all targets is

$$p_{++} = \binom{N}{2} \frac{1}{2^{2p}} \quad (\text{F1})$$

where the first term counts the number of ways of selecting two components out of the N , and the second corresponds to the probability that both components are present in all p targets. We are interested in the behavior of p_{++} when $p, N \rightarrow \infty$. In this limit, we can write $p_{++} \approx \exp(-\zeta)$ with $\zeta = -2 \log(N) + 2p \log(2)$. Calculating when this probability approaches zero, determines when the minima of the functional are exclusively corners. We find that this occurs for $p > \log(N)/\log(2)$, as initially claimed.

Appendix G: Limit of sparse targets $q \rightarrow 0$

We discuss chemical and mechanical equilibrium conditions for retrieval states in the limit of $q \approx 0$ and for $v_3 \approx 0$. The main finding of this Appendix is that also in the sparse limit of $q = 0$ a finite $v_3 > 0$ is required to stabilize retrieval states. An analogous analysis applies for $q \approx 1$.

1. Chemical equilibrium

To take the limits $q \rightarrow 0$ and $v_3 \rightarrow 0$, we make the substitution

$$\hat{a}_* = \frac{a_*}{\sqrt{q}}, \quad (\text{G1})$$

in Eqs. (B4) and (C1), and consider the expansions

$$\hat{a}_* = \hat{a}_*^{(0)} + v_3 \hat{a}_*^{(1)} + O(v_3^2) \quad (\text{G2})$$

and

$$\rho_* = \rho_*^{(0)} + v_3 \rho_*^{(1)} + O(v_3^2). \quad (\text{G3})$$

For the densities we get the coefficients

$$\rho_*^{(0)} = \frac{1}{1 + e^{-\mu_N}} \quad (\text{G4})$$

and

$$\rho_*^{(1)} = -\frac{e^{-\mu_N}}{2(1 + e^{-\mu_N})^4}. \quad (\text{G5})$$

Note that in the limit of sparse target states, the densities do not depend on the overlap \hat{a}_* , and hence retrieval regions are enriched in a few components, but their overall density will not differ from the exterior density. Also, note that the correction term $\rho_*^{(1)}$ is negative as v_3 quantifies the strength of a repulsive potential.

For the overlap parameter, we need to solve the following implicit equation

$$\hat{a}_*^{(0)} = \exp(\hat{a}_*^{(0)} \hat{v}_2) - 1, \quad (\text{G6})$$

where $\hat{v}_2 = v_2/(1 + e^{-\mu_N})$. Apart from the trivial solution $\hat{a}_*^{(0)} = 0$, Eq. (G6) admits the solution

$$\hat{a}_*^{(0)} = \begin{cases} -1 - \frac{1}{\hat{v}_2} W_{-1}(-e^{-\hat{v}_2} \hat{v}_2) & \text{if } \hat{v}_2 \leq 1, \\ -1 - \frac{1}{\hat{v}_2} W_0(-e^{-\hat{v}_2} \hat{v}_2) & \text{if } \hat{v}_2 > 1, \end{cases} \quad (\text{G7})$$

where $W_0(x)$ is the principal branch of the Lambert-W function that solves $x = W e^W$, and $W_{-1}(x)$ is the second branch of the Lambert-W function. The coefficient for the linear term in perturbation theory is given by

$$\begin{aligned} \hat{a}_*^{(1)} &= \hat{a}_*^{(0)} \frac{e^{-\mu_N + \hat{a}_*^{(0)} \hat{v}_2}}{2(1 + e^{-\mu_N})^4} \\ &\times \frac{4 + 2\hat{a}_*^{(0)} + v_2 + 2(2 + \hat{a}_*^{(0)}) \cosh(\mu_N)}{(-1 + \hat{v}_2 e^{\hat{a}_*^{(0)} \hat{v}_2})}. \end{aligned} \quad (\text{G8})$$

Note that when $\hat{a}_*^{(0)} = 0$, $\hat{a}_*^{(1)}$ is in general not zero-valued, as the denominator also converges to zero in this limit, yielding a finite value for $\hat{a}_*^{(1)}$.

In Fig. 7 we plot \hat{a}_* as a function of \hat{v}_2 up to linear order in perturbation theory. Observe that $\hat{a}_*^{(0)}$ is positive for $\hat{v}_2 < 1$ and negative for $\hat{v}_2 > 1$, while for $v_3 > 0$ the transition point where \hat{a}_* changes sign is larger than one. Interestingly, for $\hat{v}_2 \rightarrow 0$ the overlap \hat{a}_* diverges.

2. Mechanical equilibrium

Having determined the chemically stable retrieval states in the limit of sparse patterns, we now determine their mechanically stable branches. To this aim, we expand the coefficients c_1 and c_2 that appear in the stability conditions (D14) and (D15) in v_3 , viz.,

$$c_1 = c_1^{(0)} + v_3 c_1^{(1)} + O(v_3^2) \quad (\text{G9})$$

and

$$c_2 = c_2^{(0)} + v_3 c_2^{(1)} + O(v_3^2) \quad (\text{G10})$$

and we determine the above four coefficients from expanding the Eqs. (D3) and (D4) defining c_1 and c_2 and taking the limit $q \rightarrow 0$.

For the zero-order coefficients, that determine stability at $v_3 = 0$, we get

$$c_1^{(0)} = 1 + e^{-\mu_N} \quad (\text{G11})$$

and

$$c_2^{(0)} = \frac{\hat{a}_*^{(0)}}{1 + \hat{a}_*^{(0)}} (1 + e^{-\mu_N}). \quad (\text{G12})$$

Substitution of Eqs. (G11) and (G12) into Eqs. (D14) and (D15), we find that retrieval states are *not* mechanically stable for all values of \hat{v}_2 at $v_3 = 0$. Indeed, for $\hat{v}_2 \leq 1$ it holds that $\hat{a}_*^{(0)} > 0$, and therefore $c_2^{(0)} > 0$. Consequently, the inequality (D15) determines mechanical stability, which reads here $\hat{a}_*^{(0)} \leq (1 - \hat{v}_2)/\hat{v}_2$, and is not satisfied for $\hat{v}_2 \leq 1$. Analogously, for $\hat{v}_2 \geq 1$ it holds that $\hat{a}_*^{(0)} < 0$, and therefore $c_2^{(0)} < 0$. Consequently, we require the inequality (D14) that reads $\hat{v}_2 \leq 1$ in the limit $q \rightarrow 0$.

Taken together, retrieval states are not stable for $v_3 = 0$, and we require a nonzero v_3 to stabilise them. The linear-order coefficients in Eqs. (G11) and (G12) read

$$c_1^{(1)} = \frac{2 + 3e^{-\mu_N}}{2(1 + e^{-\mu_N})^2} \quad (\text{G13})$$

and

$$\begin{aligned} c_2^{(1)} &= \frac{e^{-\mu_N}}{2(1 + \hat{a}_*^{(0)})^2 (1 + e^{\mu_N})^2} \\ &\times \left(2\hat{a}_*^{(1)} (1 + e^{\mu_N})^3 \right. \\ &\left. - \hat{a}_*^{(0)} (1 + \hat{a}_*^{(0)}) e^{2\mu_N} \left\{ 1 + 2\hat{a}_*^{(0)} + 2(1 + \hat{a}_*^{(0)}) e^{\mu_N} \right\} \right). \end{aligned} \quad (\text{G14})$$

Substitution of (G11) and (G13) in (D3), and substitution of (G12) and (G14) in (D4), yields expressions for c_1 and c_2 up to linear order in v_3 , which we can substitute in Eqs. (D14) and (D15) to determine the mechanical stability of retrieval states up to linear order in perturbation theory. In Fig. 7, we depict the stable branches of the retrieval state with thick lines, demonstrating that stable retrieval is possible at small values of v_2 when $v_3 > 0$.

In Fig. 8 we plot the lines of marginal stability up to linear order in v_3 . Above these lines, the retrieval state is stable. Importantly, for finite values of v_2 we require a finite v_3 to render retrieval states mechanically stable. Note that according to Fig. 8 stable retrieval states are not possible for large enough values of v_2 , as

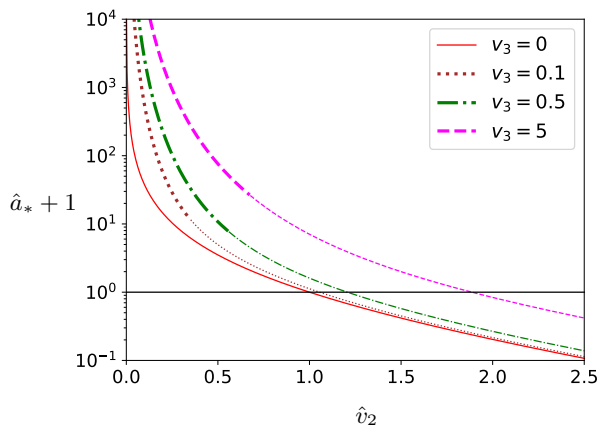


FIG. 7. Plot of the chemically stable value of the overlap $\hat{a}_* = a_*/\sqrt{q}$ of retrieval states at $q = 0$ as a function of $\hat{v}_2 = v_2/(1 + \exp(-\mu_N))$ for small values of v_3 . We used the perturbation theory up to linear order (G2) with coefficients determined by the formulae (G7) and (G8). We have set $\mu_N = 1$ and v_3 is given as in the legends. The thick lines and thin lines denote the mechanically stable and unstable branches, respectively. For $v_3 = 0$ the retrieval state is unstable for all values of \hat{v}_2 . The solid horizontal line denotes $\hat{a}_* = 0$ and is a guide to the eye.

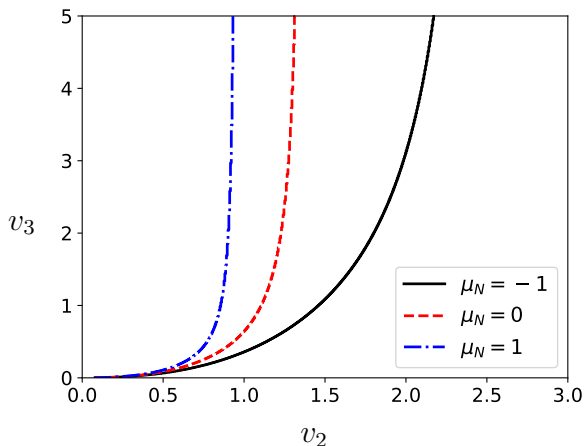


FIG. 8. Lines of marginal stability separating a stable retrieval state at large values of v_3 from an unstable retrieval state at small values of v_3 , calculated up to linear order in perturbation theory (v_3 being the small parameter).

an infinitely large v_3 is required to stabilise states beyond a finite value of v_2 . However, it should be stressed that this is a perturbative result up to linear orders in v_3 , and we expect this effect to disappear when considering higher orders in perturbation theory.

Appendix H: Numerical methods

This section outlines the numerical methods used throughout the paper.

The chemical equilibrium conditions in Eq.(13) (shown explicitly in Fig.3) are solved numerically using *Scipy Optimize least_squares* function. This function solves the non-linear system of equations by minimizing the sum of the residuals squared. Variables are bounded to their physical domains.

The stability boundaries in Fig. 2 are obtained by solving numerically the equalities in Eqs. (14) and (15). The function *fsolve* from *Scipy Optimize* is used. Parameters a_* and ρ_* are obtained as described before. For Fig. 6(D) the same approach is used for the corresponding equations (D14), (D15).

In Figs. 4, 5, 6(A) and (B), the metastable states of the mixture are obtained by minimising the extended potential $\omega(\{\rho_i\})$ with respect to ρ_i . The minimization algorithm used is a truncated Newton method. We use the *TNC* algorithm found in *Scipy Optimization library*. This is a hessian-free method which guarantees that the search direction is a descent direction and allows to bound the variables to their physical domains. For Fig.4, the initial state is a perturbed target state, where a fraction of components is set to the homogeneous value. The set of components to be perturbed is determined by a random uniform distribution. For Fig.5, the initial states are generated from random uniform Dirichlet distributions. For Fig. 6 the initial state is constructed from the *ansatz* in Eq. (12) where a_* and ρ_* are obtained as described before.

-
- [1] R. P. Sear and J. A. Cuesta, Physical review letters **91**, 245701 (2003).
 - [2] A.-C. Gavin, M. Bösche, R. Krause, P. Grandi, M. Marzioch, A. Bauer, J. Schultz, J. M. Rick, A.-M. Michon, C.-M. Cruciat, *et al.*, Nature **415**, 141 (2002).
 - [3] P. Sartori and S. Leibler, Proceedings of the National Academy of Sciences **117**, 114 (2020).
 - [4] C. P. Brangwynne, C. R. Eckmann, D. S. Courson, A. Rybarska, C. Hoegge, J. Gharakhani, F. Jülicher, and A. A. Hyman, Science **324**, 1729 (2009).
 - [5] A. A. Hyman, C. A. Weber, and F. Jülicher, Annu. Rev. Cell Dev. Biol **30**, 39 (2014).
 - [6] J.-M. Choi, A. S. Holehouse, and R. V. Pappu, Annual review of biophysics **49**, 107 (2020).
 - [7] J. Berry, C. P. Brangwynne, and M. Haataja, Reports on Progress in Physics **81**, 046601 (2018).
 - [8] D. Lingwood and K. Simons, science **327**, 46 (2010).
 - [9] F. A. Heberle and G. W. Feigenson, Cold Spring Harbor perspectives in biology **3**, a004630 (2011).
 - [10] A. Murugan, Z. Zeravcic, M. P. Brenner, and S. Leibler, Proceedings of the National Academy of Sciences **112**, 54 (2015).

- [11] W. M. Jacobs and D. Frenkel, The Journal of chemical physics **139**, 024108 (2013).
- [12] W. M. Jacobs and D. Frenkel, Biophysical journal **112**, 683 (2017).
- [13] G. Carugno, I. Neri, and P. Vivo, Physical Biology **19**, 056001 (2022).
- [14] M. Girard, Physical Biology **20**, 016006 (2022).
- [15] F. C. Thewes, M. Krüger, and P. Sollich, Phys. Rev. Lett. **131**, 058401 (2023).
- [16] D. Zwicker and L. Laan, Proceedings of the National Academy of Sciences **119**, e2201250119 (2022).
- [17] W. M. Jacobs, Physical review letters **126**, 258101 (2021).
- [18] J. J. Hopfield, Proceedings of the national academy of sciences **79**, 2554 (1982).
- [19] H. B. Callen, "Thermodynamics and an introduction to thermostatistics," (1998).
- [20] S. Safran, *Statistical Thermodynamics Of Surfaces, Interfaces, And Membranes* (CRC Press., 2003).
- [21] M. Doi, *Soft matter physics* (Oxford University Press, 2013).
- [22] S. Mao, D. Kuldinow, M. P. Haataja, and A. Košmrlj, Soft Matter **15**, 1297 (2019).
- [23] J. Hertz, A. Krogh, and R. G. Palmer, *Introduction to the theory of neural computation* (CRC Press, 2018).
- [24] K. Shrinivas and M. P. Brenner, Proceedings of the National Academy of Sciences **118**, e2108551118 (2021).
- [25] I. R. Graf and B. B. Machta, Phys. Rev. Res. **4**, 033144 (2022).
- [26] P. S. G. Carugno, R. Braz Teixeira and I. Neri, in preparation (2024).
- [27] K. G. Murty and S. N. Kabadi, *Some NP-complete problems in quadratic and nonlinear programming*, Tech. Rep. (1985).
- [28] P. M. Pardalos and G. Schnitger, Operations Research Letters **7**, 33 (1988).
- [29] P. M. Pardalos and S. A. Vavasis, Journal of Global optimization **1**, 15 (1991).
- [30] B. Kramer and A. MacKinnon, Reports on Progress in Physics **56**, 1469 (1993).
- [31] K. Efetov, *Supersymmetry in disorder and chaos* (Cambridge university press, 1999).
- [32] K. Simons and D. Toomre, Nature reviews Molecular cell biology **1**, 31 (2000).
- [33] P. A. Chong and J. D. Forman-Kay, Current opinion in structural biology **41**, 180 (2016).
- [34] Y. Shin and C. P. Brangwynne, Science **357**, eaaf4382 (2017).
- [35] S. F. Banani, H. O. Lee, A. A. Hyman, and M. K. Rosen, Nature reviews Molecular cell biology **18**, 285 (2017).
- [36] M. Mézard, G. Parisi, and M. A. Virasoro, *Spin glass theory and beyond: An Introduction to the Replica Method and Its Applications*, Vol. 9 (World Scientific Publishing Company, 1987).
- [37] P. Charbonneau, E. Marinari, G. Parisi, F. Ricci-Tersenghi, G. Sicuro, F. Zamponi, and M. Mezard, *Spin Glass Theory and Far Beyond: Replica Symmetry Breaking after 40 Years* (World Scientific, 2023).
- [38] B. Müller, J. Reinhardt, and M. T. Strickland, *Neural networks: an introduction* (Springer Science & Business Media, 1995).
- [39] D. Bollé, T. M. Nieuwenhuizen, I. P. Castillo, and T. Verbeiren, Journal of Physics A: Mathematical and General **36**, 10269 (2003).
- [40] P. N. McGraw and M. Menzinger, Phys. Rev. E **67**, 016118 (2003).
- [41] P. N. McGraw and M. Menzinger, Phys. Rev. E **67**, 016119 (2003).
- [42] A. Hedayat and W. D. Wallis, The Annals of Statistics , 1184 (1978).